Desalination and Water Treatment
www.deswater.com

(2022) 1–9

doi: 10.5004/dwt.2022.28938

Porous cellulose beads intercalated with calcium carbonate nanoparticles for dye adsorption

Jia Xin Yap, Wei Chee Gan, C.P. Leo*

School of Chemical Engineering, Engineering Campus, Universiti Sains Malaysia, 14300, Nibong Tebal, Pulau Pinang, Malaysia, email: chcpleo@usm.my (C.P. Leo)

Received 25 March 2022; | Accepted 21 September 2022

ABSTRACT

About 200,000 tonnes of dye waste is generated annually, polluting our water resources. Dye adsorption using biodegradable cellulose is of great interest because cellulose is abundantly available at a low cost, and secondary pollution can be prevented. In this study, porous cellulose beads (PCBs) were synthesised and characterised for methylene blue (MB) dye removal. The effects of calcium carbonates ($CaCO_3$) nanoparticles on PCBs properties and MB dye removal were further studied. PCBs with varied amounts of $CaCO_3$ nanoparticles (0.01, 0.03 and 0.05 wt.%) were successfully synthesised through phase inversion. The Brunauer–Emmett–Teller surface area increased from 2.67 to 12.83 m^2/g. The dye removal efficiency (R) increased from 88.12% to 97.04% at the adsorbent dosage of 0.06 g and equilibrium time of 3 h when the 0.05 wt.% of $CaCO_3$ nanoparticles were incorporated. The adsorption kinetics could be described using pseudo-second-order with R^2 values of higher than 0.99 since the adsorption process is governed by chemisorption. The maximum adsorption capacity of PCBs with 0.05 wt.% of $CaCO_3$ nanoparticles loading determined by pseudo-second-order was 49.02 mg/g. After six cycles of adsorption–desorption processes, about 50% of the dye can still be adsorbed.

Keywords: Adsorption; Calcium carbonate; Desorption; Dye; Porous cellulose bead

1. Introduction

Cellulose is the most abundant biopolymer since it can be extracted from a wide range of sources such as plants, biorefinery waste, algae, and more. In addition, nanocellulose and cellulose derivatives have been widely used as the building blocks of filters, membranes and adsorbents for wastewater treatment. These sustainable polymers offer lightweight, large surface area, great hydrophilicity, and high flexibility in chemical modification for achieving satisfactory removal of water pollutants.

Unlike other adsorbents, porous cellulose beads (PCBs) could be easily produced using the NaOH/urea aqueous solution at low temperature as the solvent, while acidic or salt solution could be used to solidify the droplets. The PCBs could attain surface area up to 99.80 m^2/g and a maximum adsorption capacity of 48.80 mg·MB/g (MB – methylene blue) [1]. Further oxidation treatment under microwave irradiation, the surface area increased to 132.27 m^2/g and the adsorption capacity improved to 873 mg/g due to the improvement of carboxylate content [2]. Adding the natural clay, sepiolite into NaOH/urea aqueous solution containing cellulose to form composite beads, the maximum adsorption capacity of malachite green of 314.47 mg/g could be achieved [3]. Harada et al. [4] incorporated activated carbon into cellulose beads which were prepared from cellulose acetate and then deacetylated through alkaline treatment. The activated carbon increased the surface area of cellulose beads from 25 to 700 m^2/g and the adsorption capacity of toluidine blue to 123.5 mg/g. Cellulose/graphene

* Corresponding author.

1944-3994/1944-3986 © 2022 Desalination Publications. All rights reserved.

oxide beads were produced using NaOH solution at –12°C as the solvent and HNO_3 solution containing NaCl as the coagulation bath for the adsorption of malachite green up to 17.862 mg/g [5]. Microcrystalline cellulose and cellulosic products were used as adsorbents for removing a cationic dye from an aqueous solution with an adsorption capacity of 82 mg/g [6,7]. Poly(vinyl alcohol) hydrogel containing TEMPO-oxidized cellulose showed an excellent adsorption of 357.140 mg·Cu^{2+}/g of hydrogel [8]. Graphene nanosheets with a large surface area (750 m^2/g) could be added into cellulose doped solution before regeneration as well [9]. The adsorption capacity increased from 98.1 to 139.6 mg·-Congo red/g after incorporating graphene nanosheet.

Cellulose/chitosan beads were synthesised using [Emim]Ac ionic liquid at 70°C as the solvent and ethanol as the coagulation bath [10]. A maximum adsorption capacity of 40 mg·Congo red/g was achieved using cellulose/chitosan beads with a surface area of 2.28377 m^2/g. Liu et al. [11] added chitosan into NaOH/urea/H_2O containing cellulose before regeneration into hydrogel beads. The hydrogel beads were crosslinked using genipin and then grafted with dimethyldiallylammonium chloride. A very low surface area of 0.73 m^2/g was recorded, but the swelling degree increased from 1.17 to 10.35 g/g after grafting. Protonated amino and quaternary ammonium groups interacted with the sulfonate groups of dyes, resulting in adsorption of Reactive red 195 and Methyl orange up to 133.52 and 190.48 mg/g, respectively. Porous cellulose beads could be prepared through the reductive amination crosslinking of 2,3-dialdehyde cellulose and chitosan [12]. Surface area increased from 8.93 ± 0.23 m^2/g to 79.67 ± 0.31 m^2/g after treatment with NaOH and diethyl ether, with adsorption capacity of 200 mg·Congo red/g recorded at pH 2. The loading of cellulose nanocrystal with a large surface area near 500 m^2/g in the alginate beads caused a maximum adsorption capacity of 256.41 mg·MB/g [13]. The mixture of nanofibrillated cellulose and alginate in an aqueous solution containing graphene oxide was dropped into $CaCl_2$ solution to form composite hydrogels with the maximum adsorption capacity of 665 mg crystal violet/g [14]. The sulfonate of lignin improved the adsorption of MB by the alginate beads containing cellulose nanocrystal with lignin near 1,181 mg/g [15].

Carboxymethyl cellulose (CMC) hydrogel could be produced from sodium carboxymethyl cellulose using a crosslinking agent or metal ions such as Cu^{2+}, Al^{3+}, and Fe^{3+}. Incorporating metal–organic frameworks such as ZIF-8 into CMC hydrogel did not improve the MB adsorption capacity significantly, but it allowed higher adsorption capacity to be regenerated using ethanol [16]. Yang et al. [17] modified CMC hydrogel with polyethyleneimine (PEI) that contains abundant amino groups to facilitate the adsorption of Methyl blue, nearly 450 mg/g. After crosslinking using $Al(NO_3)_3$, CMC hydrogel was immersed into PEI solution and then crosslinked again using glutaraldehyde. The hollow structure formed as $Al(OH)_3$ formed and destroyed the carboxyl-Al bonding, reducing the surface area from 67.958 m^2/g to the range of 1.560–22.297 m^2/g. Ding et al. [18] modified cellulose hydrogel beads using a similar method, also resulting in the reduction of surface area to 100.61 m^2/g. Due to electrostatic attraction and hydrogen bonding, the adsorption capacity for Methyl blue and Rose bengal (RB) increased to 15,550.55 and 467.95 mg/g, respectively. The carboxylated cellulose nanocrystalline/MnO_2 composite was first prepared through in situ oxidation, followed by blending into alginate solution and crosslinking in $CaCl_2$ solution to form catalytic adsorbent [19]. A maximum dye removal MB blue.

Besides co-polymers, inorganic nanoparticles were incorporated into cellulose-based adsorbents. Calcium carbonates ($CaCO_3$) nanoparticles were used as the pore templating agent in the preparation of magnetic cellulose beads from microcrystalline cellulose and Fe_3O_4 mixture in 1-butyl-3-methylimidazolium chloride ([BMIM]Cl) ionic solution [20]. The mixture was dropped into HCl solution, washed and frozen at –10°C before freeze-drying at –10°C. $CaCO_3$ nanoparticles were removed using the acidic solution, improving surface area from 5.14 to 9.10 m^2/g. The subsequent modification using glutaric anhydride improved the maximum adsorption capacity to 1,186.8 mg·MB/g and 151.8 mg·Rhodamine B/g. Similarly, $CaCO_3$ was added into the mixture of cellulose and oxalic acid modified montmorillonite in NaOH/urea solution as the template [21]. The surface area increased from 28.8 to 46.0 m^2/g when 30 wt.% of $CaCO_3$ was incorporated, but the pore collapsed at higher loading of $CaCO_3$. Unlike previous works, $CaCO_3$ nanoparticles were incorporated into cellulose beads as the additional adsorption sites in this study. Biocompatible $CaCO_3$ nanoparticles were incorporated into cellulose dope solution before synthesising PCBs through phase inversion. The effects of $CaCO_3$ nanoparticles on the morphology and dye removal efficiency of PCBs were examined.

2. Materials and methods

2.1. Materials

α-cellulose (>97%) from Sigma Life Science was used as the major building block of PCBs. Other chemicals such as sodium hydroxide (NaOH) (>99%, Merck), urea (>99.5%, Merck), ethanol (absolute, Merck), MB (Reag. Ph Eur, Merck), calcium carbonate ($CaCO_3$) nanoparticles (≥98%, Shanghai Manufacturer), and calcium chloride ($CaCl_2$) (>97%, Sigma-Aldrich) were used without further purification. $CaCO_3$ nanoparticles (40–80 nm) were acquired from XFNANO (China).

2.2. Synthesis and characterisation of PCBs incorporated with $CaCO_3$ nanoparticles

NaOH/urea aqueous solution was used as the solvent to prepare the cellulose dope solution. NaOH, urea, and distilled water were first mixed at a weight ratio of 6:4:100 and then stored in a refrigerator at –12°C. Subsequently, 5 g of α-cellulose was dispersed into 100 mL of NaOH/urea aqueous solution to form the dope solution with a cellulose concentration of 5 wt.%. The mixture was stirred vigorously at 1,200 rpm for 10 min until all the α-cellulose was dispersed. The dissolution of cellulose was repeated for the preparation of the dope solution containing $CaCO_3$ nanoparticles (0.01, 0.03 and 0.05 wt.%). The dope solution was degassed using a planetary mixer-deaerator (Kurabo Mazerustar, KK-300SS) at 1,500 rpm for 1 min. PCBs with a diameter

of approximately 2.5 mm were continuously produced by dropping the dope solution into $CaCl_2$ solution (5 wt.%) using a modified syringe with a needle diameter of 0.8 mm. The height between the needle tip and the bath surface was fixed at 24 cm, as shown in Fig. S1. The PCBs formed were further washed with distilled water at least 10 times to eliminate NaOH/urea solution and $CaCl_2$ until reaching neutral pH. The PCBs were frozen at –10°C for 12 h and then immersed in ethanol for about 2 h before being frozen again in an ultra-low temperature freezer (Sanyo VIP Plus Ultra Low Ing Climas, CVF525/86) at –48°C for overnight. The frozen PCBs were freeze-dried under vacuum in the freeze dryers (Labconco) at 48°C for 48 h.

The Fourier-transform infrared (FTIR) spectra of the PCBs were recorded using an FTIR spectrometer (Nicolet™ iS20, Thermo Fisher Scientific Inc.) equipped with a deuterated triglycine sulphate detector (DTGS) and a versatile attenuated total reflectance (ATR) accessory. FTIR spectra were obtained within the range between 4,000 and 650 cm^{-1} and 32 sample/background scans at a resolution of 0.25 cm^{-1}. The cross-section of the PCBs was examined using a scanning electron microscope (SEM, Hitachi Model TM3000). The crystallinity of $CaCO_3$ in the cellulose matrix was studied using X-ray diffraction (XRD) patterns collected from an automated X-ray diffractometer system (D8 Advance, Bruker, Karlsruhe, Germany) with Cu-Kα radiation (15.4056 nm) at 40 kV and 40 mA. The N_2 adsorption–desorption isotherms were collected after degassing PCBs at 150°C for 6 h under N_2 flow (Micromeritics ASAP 2020). The specific surface area, Langmuir surface area, t-plot, Barrett–Joyner–Halenda (BJH) adsorption, BJH desorption and total pore volume of PCBs were determined.

2.3. Dye adsorption

Before conducting the adsorption test, a calibration curve to determine MB concentration was established according to Beer's law. The light intensity of samples with different concentrations was recorded at a wavelength of 665 nm using a UV-Vis Spectrophotometer (Cary 60, Agilent). Then, adsorption experiments were performed by adding 4 mg of PCBs into 20 mL of MB solution with a concentration of 10 ppm. The mixture was shaken at 100 rpm using an orbital laboratory shaker (Major Science, MS-NOR-30). The dye concentration at different time intervals was determined using a UV-Vis Spectrophotometer (Cary 60, Agilent) at a wavelength of 665 nm. The adsorption capacity (Q_e, mg/g) and the removal efficiency (R, 100%) were determined using Eqs. (1) and (2):

$$Q_e = \left(C_o - C_e\right)\frac{V}{M} \tag{1}$$

$$R = \frac{\left(C_o - C_e\right)}{C_o} \times 100\% \tag{2}$$

where C_o (mg/L) is the initial dye concentration of MB, C_e (mg/L) is the equilibrium dye concentration of MB, V (L) is the volume of the dye solution, and M (mg) is the weight of PCBs. The adsorption kinetics were further studied by fitting the pseudo-first-order [Eq. (3)], pseudo-second-order [Eq. (4)], and intraparticle diffusion [Eq. (5)] models.

$$\ln\left(Q_e - Q_t\right) = \ln Q_e - k_1 t \tag{3}$$

$$\frac{t}{Q_t} = \frac{1}{k_2 Q_e^2} + \frac{t}{Q_e} \tag{4}$$

$$Q_t = k_{\text{di}} t^{1/2} + C_i \tag{5}$$

where Q_t (mg/g) is the adsorption capacity at a given time t (h), k_1 (h^{-1}) is the rate constant of pseudo-first-order kinetics equation, k_2 ($g/mg{\cdot}h^{0.5}$) is the rate constant of pseudo-second-order kinetics equation, k_{di} ($g/mg{\cdot}h^{0.5}$) is the intraparticle rate constants, and C_i (mg/g) represents the adsorption constant which is the intercept value.

In the regeneration tests, 1 g of PCBs were added into 50 mL MB solution with a concentration of 100 mg/L at pH 7. After 3 h, the MB-loaded PCBs were immersed in 10 mL of hydrochloric acid (HCl) solution (0.15 M) for 15 min under 120 rpm at 25°C. The desorption efficiency was determined.

$$\text{Desorption efficiency } (\%) = \frac{C_{\text{desorbed}}\left(\frac{\text{mg}}{\text{L}}\right)}{C_{\text{adsorbed}}\left(\frac{\text{mg}}{\text{L}}\right)} \times 100\% \tag{6}$$

where C_{desorbed} is the final MB concentration in desorption medium and C_{adsorbed} is the MB concentration of MB adsorbed by PCBs.

3. Results and discussion

3.1. Characteristics of PCBs incorporated with $CaCO_3$ nanoparticles

Fig. 1 shows the FTIR spectra of PCBs, PCBs/0.01 wt.% $CaCO_3$, PCBs/0.03 wt.% $CaCO_3$ and PCBs/0.05 wt.% $CaCO_3$. All the FTIR spectra showed an intense and broad adsorption band at 3,335 cm^{-1} due to the stretching vibration of –OH groups. The peaks located at 2,890 cm^{-1} could be related to the stretching vibration of –CH group. The other bands at 1,637 and 1,407 cm^{-1} represent the –OH bending of absorbed water and bending vibration of –CH group, respectively. The spectra pattern is similar to the FTIR spectra of cellulose-based membrane scaffolds [22], and regenerated cellulose thin films [23] prepared using NaOH/urea aqueous solution as the solvent. The bands at 1,155 cm^{-1} correspond to the stretching vibration of the C–O–C bond in cellulose, while the peaks around 1,019 cm^{-1} represent the skeletal vibration of the C–O–C pyranose ring in cellulose [24]. The band at 872 cm^{-1} could be related to the bending of CO_3^{2-} due to the presence of calcite, which is the most stable polymorph of $CaCO_3$ [25,26]. By increasing the $CaCO_3$ loading, the band absorbance increased [27]. The increasing absorbance of CO_3^{2-} band at 1,407 cm^{-1}

and the cellulose peak at 1,019 cm^{-1} in the FTIR spectra also indicated the good dispersion of $CaCO_3$ nanoparticles on the cellulose matrix [26,27]. The FTIR spectra of PCBs samples was comparable to that of commercial cellulose [28], demonstrating no cellulose degradation after dissolution in NaOH/urea aqueous solution.

For the formation of cellulose spheres, cellulose dope solution was added into $CaCl_2$ dropwise to initiate the precipitation. The dropping was more likely to form the elliptical shape due to the mechanical distortion of droplets when they stroke the surface of a coagulation bath [29]. PCBs were then frozen before being freeze-dried. After freeze-drying, the interconnected pores were created due to the presence of small ice particles in PCBs during freezing. Fig. 2 shows the SEM images of porous PCBs, namely (a) PCBs, (b) PCBs/0.01 wt.% $CaCO_3$, (c) PCBs/0.03 wt.% of $CaCO_3$, and (d) PCBs/0.05 wt.% of $CaCO_3$.

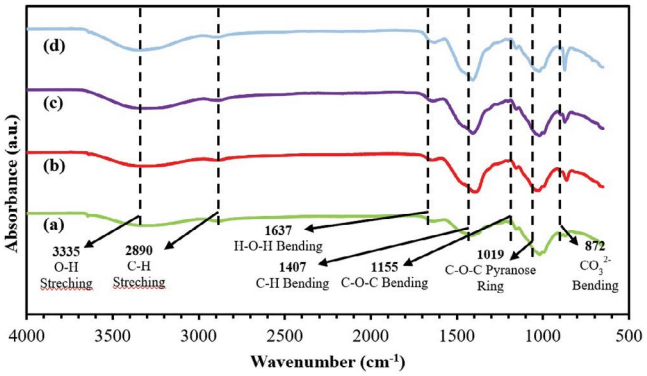

Fig. 1. FTIR spectra (a) PCBs, (b) PCBs/0.01 wt.% $CaCO_3$, (c) PCBs/0.03 wt.% $CaCO_3$, and (d) PCBs/0.05 wt.% $CaCO_3$ samples.

The PCBs consist of randomly oriented and twisted cellulose fibers, as reported by others [30,31]. The NaOH/urea aqueous solution disrupted the inter and intra-cellulose connections, causing cellulose to rearrange to form a porous structure [32]. Larger pores formed inside PCBs when the $CaCO_3$ amount was increased from 0 to 0.05 wt.% [1]. The hydrophilic $CaCO_3$ nanoparticles enhanced the demixing rate during phase inversion and pore formation. The large pores were expected to promote molecule diffusion within the adsorbents and interaction with carboxylate groups [22]. Differently, [33] used ethanol bath to prolong the demixing process for promoting the growth of pores. $CaCO_3$ nanoparticles were also helpful to reduce pore collapse and to increase the surface area after freeze-drying [34].

The crystallinity changes after incorporating $CaCO_3$ into PCBs are shown in Fig. 3. The XRD patterns of PCBs and PCBs/0.05 wt.% $CaCO_3$ samples exhibited diffraction peaks of cellulose II at 2θ around 11.2°, 20.0° and 21.7°, corresponding to the (1 1 0) and (0 2 0) planes, respectively [35]. The cellulose structure was successfully preserved during the formation of beads. The XRD peaks of PCBs/0.05 wt.% $CaCO_3$ sample located at 2θ of 29.7°, 34.5°, 39.9°, 43.9°, 47.2° and 48.5° could be assigned to the plane of calcite [36,37]. The more intense and sharp peaks for cellulose II indicated that the precipitate $CaCO_3$ generated a further disordered arrangement of cellulose chains while maintaining the high crystallinity of calcite in PCBs.

The nitrogen adsorption–desorption isotherms were analysed to determine the surface area, pore volume and pore diameter of PCBs samples, as summarised in Table 1. The Brunauer–Emmett–Teller (BET) surface area increased from 2.67 to 12.83 m^2/g, while the BJH adsorption pore volume increased from 0.0041 to 0.0103 cm^3/g when the $CaCO_3$ loading was raised to 0.05 wt.%. However, the average pore diameter decreased from 55.00 to 7.15 nm, indicating the formation of mesopores [38]. This improvement could

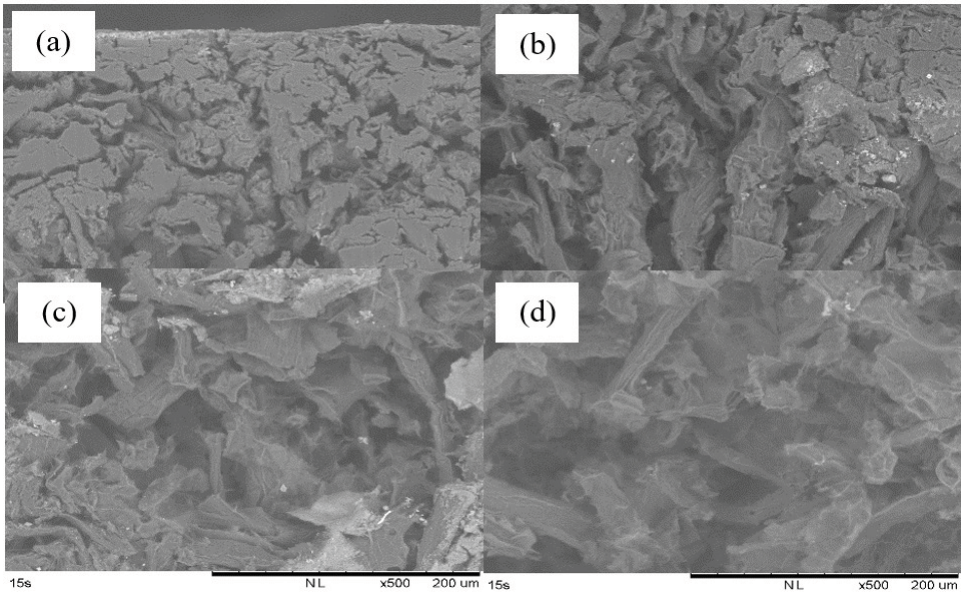

Fig. 2. SEM images shows the cross-section of (a) PCBs, (b) PCBs/0.01 wt.% $CaCO_3$, (c) PCBs/0.03 wt.% $CaCO_3$, and (d) PCBs/0.05 wt.% $CaCO_3$ samples.

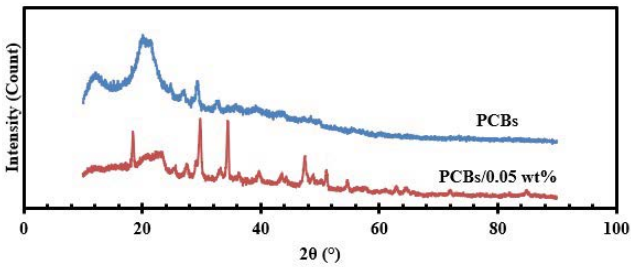

Fig. 3. XRD patterns of (a) PCBs and (b) PCBs/0.05 wt.% $CaCO_3$ samples.

Table 1
BET surface area, pore volume and pore diameter for PCBs, PCBs/0.01 $CaCO_3$, PCBs/0.03 $CaCO_3$ and PCBs/0.05 $CaCO_3$

Sample	BET surface area (m^2/g)	Pore volume (cm^3/g)[a]	Pore diameter (nm)[b]
PCBs	2.67	0.0041	55.00
PCBs/0.01 wt.% $CaCO_3$	2.20	0.0044	13.34
PCBs/0.03 wt.% $CaCO_3$	1.95	0.0058	38.91
PCBs/0.05 wt.% $CaCO_3$	12.83	0.0103	7.15

[a]BJH adsorption cumulative volume of pore.
[b]BJH absorption average pore diameter.

be related to the improvement of pore formation caused by $CaCO_3$ nanoparticles. In addition, $CaCO_3$ nanoparticles provided additional adsorption sites and surface area besides improving the intercalation of cellulose fibers [39]. In comparison to PCBs, the BET surface area of PCBs/0.01 $CaCO_3$ and PCBs/0.03 $CaCO_3$ reduced slightly but increased dramatically up to 12.83 m^2/g for PCBs/0.05 $CaCO_3$. The addition of 0.05 wt.% of $CaCO_3$ could promote pore formation effectively, as shown in SEM images. A low $CaCO_3$ content could not promote pore formation significantly and resulted in pore blockage.

3.2. Dye adsorption on PCBs incorporated with $CaCO_3$ nanoparticles

The effects of adsorbent dosage on dye adsorption by PCBs was first investigated. Fig. 4 shows that the dye removal percentage (R) continued to rise with increasing adsorbent dosage. The rise could be related to the increment of surface area and active sites by increasing PCBs dosage. Hence, the dye removal efficiency improved from 80.47% to 88.69% as the adsorbent dosage was raised from 0.02 g to 0.04 g. It was also discovered that R-value began to decrease to 85.92% at 0.06 g. However, the adsorption capacity at equilibrium (Q_e) declined from 75.74 to 27.40 mg/g when the PCBs dosage increased from 0.02 g to 0.06 g. The decline is caused by the aggregation of accessible adsorbent surface area at high adsorbent dosage, which increased the path length of diffusion [40].

The subsequent adsorption tests using adsorbent dosage at 0.04 g. Fig. 5 shows the effect of $CaCO_3$ nanoparticles loading on dye adsorption at ambient pH and

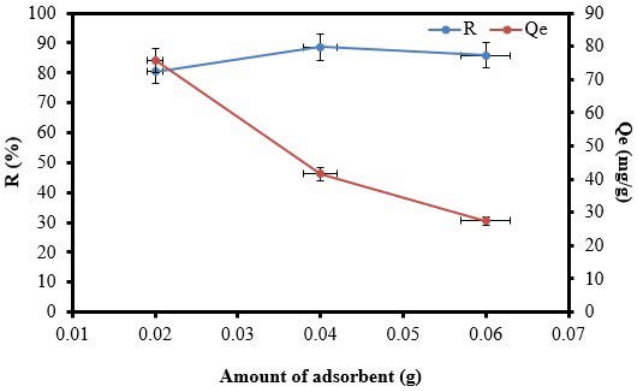

Fig. 4. Effect of adsorbent dosage on dye adsorption.

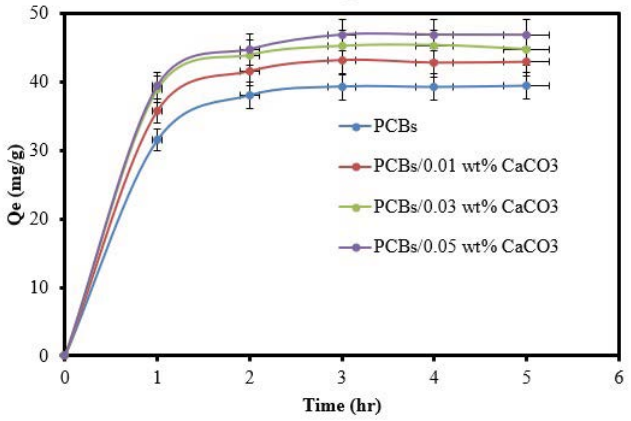

Fig. 5. Effects of $CaCO_3$ loading on dye removal using PCBs.

temperature. The cellulose beads showed the highest MB adsorption at pH 7, and the adsorption capacity decreased under acidic or basic conditions. In the acidic solution, the excess H^+ ions competed with cationic MB molecules and reduced the active surface sites for MB adsorption. As the pH increased with the addition of NaOH, chloride groups of MB reacted with sodium groups of NaOH to form sodium chloride (NaCl) salts [41,42]. Dye adsorption was considerably fast during the first hour of the adsorption process due to the availability of active sites on the adsorbent surface to achieve maximum adsorption capacity [20,41,42]. The adsorption began to slow down and eventually achieved equilibrium over time because of slow diffusion into the porous structure. The equilibrium was achieved within 3 h for the dye solution (20 mL) with an initial concentration of 10 mg/L using 0.04 g of PCBs. A similar trend was reported by [42] in the removal of MB using oil palm fronds microcrystalline cellulose. They achieved equilibrium adsorption within 60 min using 10 g of adsorbent for MB solution (25 mL) with a concentration of 10 mg/L.

As summarised in Table 2, PCBs without additives only removed MB up to 88.12%. After adding 0.01 to 0.05 wt.% of $CaCO_3$ nanoparticles into PCBs, the dye adsorption increased up to 97.05%. $CaCO_3$ nanoparticles served as an effective pore formation agent, increasing the surface area of PCBs for dye adsorption. In the preparation of cellulose/

microfibrilled cellulose composite for MB adsorption, Li et al. [43] observed the improvement in dye adsorption due to the enhanced pore formation in the presence of CO_2 generated by $CaCO_3$ in HCl solution. The content of $CaCO_3$ could not be increased beyond 0.05 wt.%. $CaCO_3$ content of 0.07 wt.% caused the dye adsorption to drop to 90.94% (Table S2). Higher $CaCO_3$ content might lead to particle agglomeration and a longer diffusion path for adsorption, resulting in a lower percentage of MB adsorption [44]. Furthermore, a high $CaCO_3$ content might cause pore blockage in PCBs [45].

Pseudo-first-order and pseudo-second-order kinetic models were used to study the surface-controlled adsorption rate in this work. As shown in Table 3, the correlation coefficient, R^2 of the pseudo-second-order kinetic model is greater than the correlation coefficient R^2 of the pseudo-first-order kinetic model. Furthermore, the adsorption capacity $Q_{e,\text{cal}}$ could be estimated close to the experimental adsorption capacity, $Q_{e,\text{exp}}$ using the pseudo-second-order equation as reported by [1,20]. The pseudo-second-order model described the MB adsorption by PCBs samples satisfactorily, showing that the rate-determining step was the chemisorption [47]. To determine the rate-limiting step using intraparticle models, MB adsorption on PCBs samples could be divided into three phases (Fig. S2). Table 3 lists the rate constants k_{di} (i = 1, 2, 3) at different phases. The adsorption rate constant in the first stage (k_{d1}) is greater than in the second (k_{d2}), and third stages (k_{d3}) because the adsorption rates at the first stage are higher than those at the second and third stages. The dye adsorption on the adsorbent surface at the first phase was only limited by the bulk diffusion, while the adsorption was limited by intraparticle diffusion at the second phase. Lastly, the adsorption at the third phase is the slowest because very few adsorption sites were accessible for the dye molecules. The observation is similar to other work by Cheung et al. [47] who commented that only one rate-limiting step could dominate the adsorption at one phase. Tan et al. [48] also further explained that boundary layer diffusion controlled the dye adsorption on microcrystalline cellulose.

The desorption performance and reusability of PCBs with 0.05 wt.% of $CaCO_3$ nanoparticles are shown in Fig. 6. In general, the adsorption capacity and desorption efficiency decreased after 6 cycles of regeneration. The desorption of MB was caused by the protonation of PCBs using HCl. The desorption freed the active sites for the following cycle of adsorption [49]. The adsorption capacity reduced from 46.52 to 36.24 mg/g, while desorption dropped from 82.6% to 75.2% after the second cycle. After 6 cycles of adsorption–desorption processes, about 50% of the dye can still be adsorbed. However, the desorption performance dropped to about 40% after 6 cycles. The drop in adsorption was caused by the accumulation of occupied sites along with the adsorption–desorption cycles [9]. In this study, cellulose fibers were stabilised by Na^+ counter-ions. The addition of HCl during the repeated desorption process could disrupt the repulsion between cellulose, causing the deterioration of active sites [50]. As a result, the total

Table 2
Dye removal percentage using PCBs with different $CaCO_3$ loading at equilibrium

Samples	Dye removal percentage (%)
PCBs (without additive of CaCO3)	88.12
PCBs/0.01 wt.% CaCO3	89.99
PCBs/0.03 wt.% CaCO3	94.05
PCBs/0.05 wt.% CaCO3	97.04

Table 3
Kinetic model constant of the pseudo-first-order and pseudo-second-order models for dye adsorption using PCBs incorporated with $CaCO_3$

Sample	Qe,exp (mg/g)	Pseudo-first-order kinetic			Pseudo-second-order kinetic		
		$Q_{e,\text{cal}}$ (mg/g)	k_1 (h^{-1})	R^2	$Q_{e,\text{cal}}$ (mg/g)	k_2 (mg/g·h)	R^2
PCBs	39.2683	17.6300	0.1218	0.6587	41.6667	0.0960	0.9985
PCBs/0.01 wt.% CaCO3	43.1338	13.4154	0.1544	0.6473	44.8430	0.1130	0.9988
PCBs/0.03 wt.% CaCO3	45.1561	10.2821	0.1749	0.6070	46.5116	0.1491	0.9989
PCBs/0.05 wt.% CaCO3	46.8117	10.6942	0.2889	0.7542	49.0196	0.1040	0.9993

Table 4
Kinetic parameters and correlation coefficient of the intraparticle diffusion model for dye adsorption using PCBs incorporated with $CaCO_3$

Sample	k_{d1} (g/mg·$h^{0.5}$)	C_1	R_1^2	k_{d2} (g/mg·$h^{0.5}$)	C_2	R_2^2	k_{d3} (g/mg·$h^{0.5}$)	C_3	R_3^2
PCBs	25.0670	1.6008	0.9533	2.0491	33.3150	0.9024	0.0554	39.0590	0.3569
PCBs/0.01 wt.% CaCO3	27.8220	1.9836	0.9425	2.1653	36.7730	0.9550	0.1275	43.4320	0.4304
PCBs/0.03 wt.% CaCO3	29.8340	2.2504	0.9361	1.7043	40.1430	0.9605	0.2379	45.9940	0.5511
PCBs/0.05 wt.% CaCO3	30.3460	2.2695	0.9371	2.3374	39.8550	0.9932	0.0129	46.8530	0.9018

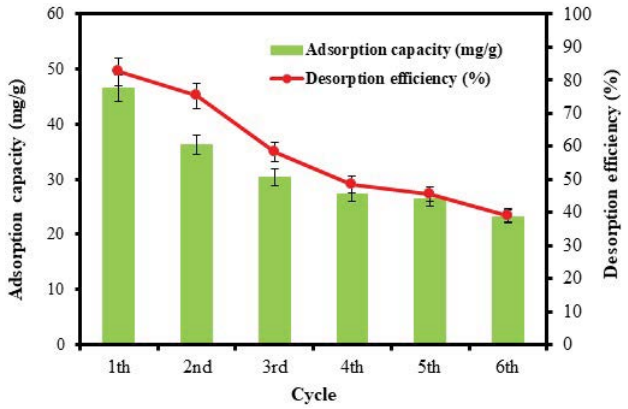

Fig. 6. Adsorption capacity of PCBs/0.05 wt.% of $CaCO_3$ on MB after regeneration.

surface area available for the consecutive adsorption cycle could be reduced. The electrostatic interaction between functional groups of adsorbents and cationic dye could also be disturbed, leading to low desorption [51]. In addition, dye molecules could be trapped inside the porous structure, causing incomplete desorption. Similar findings were reported in the study of Cu^{2+} adsorption using sodium trimetaphosphate-modified cellulose beads [52].

4. Conclusions

In this study, PCBs with varied amounts of $CaCO_3$ nanoparticles (0.01, 0.03 and 0.05 wt.%) were successfully synthesised using NaOH/urea aqueous solution as the solvent in the phase inversion process. PCBs intercalated with $CaCO_3$ nanoparticles showed enhanced porous structure. The surface area increased significantly for the improvement of adsorption capacity. $CaCO_3$ nanoparticles acted as the pore-forming agent by improving the demixing rate. PCBs with 0.05 wt.% of $CaCO_3$ nanoparticles loading attained maximum removal of MB, which was 97.04% at the adsorbent dosage of 0.04 g and equilibrium time of 3 h. The adsorption of dye by PCBs samples was well described by the pseudo-second-order kinetic model it was dominated by the chemical adsorption.

Acknowledgements

This work is the output of the ASEAN IVO (http://www.nict.go.jp/en/asean_ivo/index.html) project, IoT System for Water Reuse in Developing Cities, and financially supported by NICT (http://www.nict.go.jp/en/index.html).

Data availability statement

All relevant data are included in the paper or it's Supplementary Information.

References

[1] J. Hua, R. Meng, T. Wang, H. Gao, Z. Luo, Y. Jin, L. Liu, J. Yao, Highly porous cellulose microbeads and their adsorption for methylene blue, Fibers Polym., 20 (2019) 794–803.
[2] F. Lin, Y. You, X. Yang, X. Jiang, Q. Lu, T. Wang, B. Huang, B. Lu, Microwave-assisted facile synthesis of TEMPO-oxidized cellulose beads with high adsorption capacity for organic dyes, Cellulose, 24 (2017) 5025–5040.
[3] X. Jiang, S. Wang, L. Ge, F. Lin, Q. Lu, T. Wang, B. Huang, B. Lu, Development of organic–inorganic hybrid beads from sepiolite and cellulose for effective adsorption of malachite green, RSC Adv., 7 (2017) 38965–38972.
[4] N. Harada, J.-i. Nakamura, H. Uyama, Single-step fabrication and environmental applications of activated carbon-containing porous cellulose beads, React. Funct. Polym., 160 (2021) 104830, doi: 10.1016/j.reactfunctpolym.2021.104830.
[5] X. Zhang, H. Yu, H. Yang, Y. Wan, H. Hu, Z. Zhai, J. Qin, Graphene oxide caged in cellulose microbeads for removal of malachite green dye from aqueous solution, J. Colloid Interface Sci., 437 (2015) 277–282.
[6] D. Suteu, G. Biliuta, R. Lacramioara, S. Coseri, C. Vial, A regenerable microporous adsorbent based on microcrystalline cellulose for organic pollutants adsorption, Desal. Water Treat., 146 (2019) 176–187.
[7] I. Nica, G. Biliuta, C. Zaharia, R. Lacramioara, S. Coseri, D. Suteu, Fixed-bed-column studies for methylene blue removal by cellulose cellets, Environ. Eng. Manage. J., 19 (2020) 269–279.
[8] I. Nica, C. Zaharia, R. Baron, S. Coseri, D. Suteu, Adsorptive materials based on cellulose: preparation, characterization and application for copper ions retention, Cellul. Chem. Technol., 54 (2020) 579–590.
[9] M.E. González-López, C.M. Laureano-Anzaldo, A.A. Pérez-Fonseca, C. Gómez, J.R. Robledo-Ortíz, Congo red adsorption with cellulose-graphene nanoplatelets beads by differential column batch reactor, J. Environ. Chem. Eng., 9 (2021) 105029, doi: 10.1016/j.jece.2021.105029.
[10] M. Li, Z. Wang, B. Li, Adsorption behaviour of Congo red by cellulose/chitosan hydrogel beads regenerated from ionic liquid, Desal. Water Treat., 57 (2016) 16970–16980.
[11] Q. Liu, N. Xia, W. Wan, Y. Gao, S. Zhu, Selective capture of toxic anionic dyes of a novel prepared DMDAAC-grafted chitosan/genipin/cellulose hydrogel beads with antibacterial activity, Int. J. Biol. Macromol., 189 (2021) 722–733.
[12] C.-Q. Ruan, M. Strømme, J. Lindh, Preparation of porous 2,3-dialdehyde cellulose beads crosslinked with chitosan and their application in adsorption of Congo red dye, Carbohydr. Polym., 181 (2018) 200–207.
[13] N. Mohammed, N. Grishkewich, R.M. Berry, K.C. Tam, Cellulose nanocrystal–alginate hydrogel beads as novel adsorbents for organic dyes in aqueous solutions, Cellulose, 22 (2015) 3725–3738.
[14] H. Liu, B. Pan, Q. Wang, Y. Niu, Y. Tai, X. Du, K. Zhang, Crucial roles of graphene oxide in preparing alginate/nanofibrillated cellulose double network composites hydrogels, Chemosphere, 263 (2021) 128240, doi: 10.1016/j.chemosphere.2020.128240.
[15] M. Ma, Z. Liu, L. Hui, Z. Shang, S. Yuan, L. Dai, P. Liu, X. Liu, Y. Ni, Lignin-containing cellulose nanocrystals/sodium alginate beads as highly effective adsorbents for cationic organic dyes, Int. J. Biol. Macromol., 139 (2019) 640–646.
[16] N. Marsiezade, V. Javanbakht, Novel hollow beads of carboxymethyl cellulose/ZSM-5/ZIF-8 for dye removal from aqueous solution in batch and continuous fixed bed systems, Int. J. Biol. Macromol., 162 (2020) 1140–1152.
[17] H.-R. Yang, S.-S. Li, Q.-D. An, S.-R. Zhai, Z.-Y. Xiao, L.-P. Zhang, Facile transformation of carboxymethyl cellulose beads into hollow composites for dye adsorption, Int. J. Biol. Macromol., 190 (2021) 919–926.
[18] Y. Ding, C. Song, W. Gong, L. Liu, M. Wu, L. Li, J. Yao, Robust, sustainable, hierarchical multi-porous cellulose beads via pre-crosslinking strategy for efficient dye adsorption, Cellulose, 28 (2021) 7227–7241.
[19] H. Diao, Z. Zhang, Y. Liu, Z. Song, L. Zhou, Y. Duan, J. Zhang, Facile fabrication of carboxylated cellulose nanocrystal–MnO_2 beads for high-efficiency removal of methylene blue, Cellulose, 27 (2020) 7053–7066.

[20] B. Li, Q. Zhang, Y. Pan, Y. Li, Z. Huang, M. Li, H. Xiao, Functionalized porous magnetic cellulose/Fe_3O_4 beads prepared from ionic liquid for removal of dyes from aqueous solution, Int. J. Biol. Macromol., 163 (2020) 309–316.
[21] H. Xie, Y. Pan, H. Xiao, H. Liu, Preparation and characterization of amphoteric cellulose–montmorillonite composite beads with a controllable porous structure, J. Appl. Polym. Sci., 136 (2019) 47941, doi: 10.1002/app.47941.
[22] J.X. Yap, C.P. Leo, N.H. Mohd Yasin, C.J.C. Derek, Sustainable cultivation of *Navicula incerta* using cellulose-based scaffold incorporated with nanoparticles in air-liquid interface cultivation system, Chemosphere, 273 (2021) 129657, doi: 10.1016/j.chemosphere.2021.129657.
[23] X. Xu, J. Li, L. Ma, X. Ma, Preparation and properties of biocomposite from poly(3-hydroxybutyrate-co-3-hydroxyhexanoate) reinforced with regenerated cellulose, Cellulose, 26 (2019) 5427–5436.
[24] J.X. Yap, C.P. Leo, N.H. Mohd Yasin, P.L. Show, C.J.C. Derek, Stability evaluation and formula optimization of cellulose-based scaffold for the air-liquid interface cultivation of *Navicula incerta*, Environ. Res., 199 (2021) 111298, doi: 10.1016/j.envres.2021.111298.
[25] D. Kuo, T. Nishimura, S. Kajiyama, T. Kato, Bioinspired environmentally friendly amorphous $CaCO_{(3)}$-based transparent composites comprising cellulose nanofibers, ACS Omega, 3 (2018) 12722–12729.
[26] C. Vilela, C.S.R. Freire, P.A.A.P. Marques, T. Trindade, C. Pascoal Neto, P. Fardim, Synthesis and characterization of new $CaCO_3$/cellulose nanocomposites prepared by controlled hydrolysis of dimethylcarbonate, Carbohydr. Polym., 79 (2010) 1150–1156.
[27] L.-H. Fu, Y.-Y. Dong, M.-G. Ma, S.-M. Li, R.-C. Sun, Compare study $CaCO_3$ crystals on the cellulose substrate by microwave-assisted method and ultrasound agitation method, Ultrason. Sonochem., 20 (2013) 839–845.
[28] B. Abderrahim, E. Abderrahman, A. Mohamed, T. Fatima, T. Abdesselam, O. Krim, Kinetic thermal degradation of cellulose, polybutylene succinate and a green composite: comparative study, World J. Environ. Eng., 3 (2015) 95–110.
[29] M. Gericke, J. Trygg, P. Fardim, Functional cellulose beads: preparation, characterization, and applications, Chem. Rev., 113 (2013) 4812–4836.
[30] J. Trygg, P. Fardim, M. Gericke, E. Mäkilä, J. Salonen, Physicochemical design of the morphology and ultrastructure of cellulose beads, Carbohydr. Polym., 93 (2013) 291–299.
[31] X. Ma, C. Liu, D.P. Anderson, P.R. Chang, Porous cellulose spheres: preparation, modification and adsorption properties, Chemosphere, 165 (2016) 399–408.
[32] S.X. Shu, C.R. Li, Fabrication and characterization of regenerated cellulose/TiO_2 nanocomposite hybrid fibers, Adv. Mater. Res., 418–420 (2012) 237–241.
[33] W.-L. Tan, H.-F. Tan, A.L. Ahmad, C.P. Leo, Carbon dioxide conversion into calcium carbonate nanoparticles using membrane gas absorption, J. CO_2 Util., 48 (2021) 101533, doi: 10.1016/j.jcou.2021.101533.
[34] Y.-y. Pei, D.-m. Guo, Q.-d. An, Z.-y. Xiao, S.-r. Zhai, B. Zhai, Hydrogels with diffusion-facilitated porous network for improved adsorption performance, Korean J. Chem. Eng., 35 (2018) 2384–2393.
[35] J. Gong, J. Li, J. Xu, Z. Xiang, L. Mo, Research on cellulose nanocrystals produced from cellulose sources with various polymorphs, RSC Adv., 7 (2017) 33486–33493.
[36] Q. Zhu, J. Wang, J. Sun, Q. Wang, Preparation and characterization of regenerated cellulose biocomposite film filled with calcium carbonate by in situ precipitation, Bioresources, 15 (2020) 7893–7905.
[37] M. El-Shahate, I. Saraya, H. Hassan, A. Latif, Preparation of vaterite calcium carbonate in the form of spherical nano-size particles with the aid of polycarboxylate superplasticizer as a capping agent, Am. J. Nanomater., 4 (2016) 44–51.
[38] Y. Pan, H. Xie, H. Liu, P. Cai, H. Xiao, Novel cellulose/montmorillonite mesoporous composite beads for dye removal in single and binary systems, Bioresour. Technol., 286 (2019) 121366, doi: 10.1016/j.biortech.2019.121366.
[39] Q. Lin, Y. Wu, X. Jiang, F. Lin, X. Liu, B. Lu, Removal of bisphenol A from aqueous solution via host-guest interactions based on β-cyclodextrin grafted cellulose bead, Int. J. Biol. Macromol., 140 (2019) 1–9.
[40] N. Muchanyereyi, Removal of methylene blue from aqueous solution by dehydrated maize tassels, J. Chem. Sci., 4 (2014) 5–12.
[41] H. Ni'Mah, D. Puspitasari, A.R. Kurniawan, B. Muiz, A. Roesyadi, F. Kurniawansyah, E.O. Ningrum, Kinetic study of cationic dye adsorption on cellulose acetate butyrate/poly(L-lactic acid) composite beads, AIP Conf. Proc., 2197 (2020) 120002, doi: 10.1063/1.5140959.
[42] Y. Li, H. Xiao, M. Chen, Z. Song, Y. Zhao, Absorbents based on maleic anhydride-modified cellulose fibers/diatomite for dye removal, J. Mater. Sci., 49 (2014) 6696–6704.
[43] Y. Li, H. Xiao, Y. Pan, L. Wang, Novel composite adsorbent consisting of dissolved cellulose fiber/microfibrillated cellulose for dye removal from aqueous solution, ACS Sustainable Chem. Eng., 6 (2018) 6994–7002.
[44] A.F. Hassan, A.M. Abdel-Mohsen, M.M.G. Fouda, Comparative study of calcium alginate, activated carbon, and their composite beads on methylene blue adsorption, Carbohydr. Polym., 102 (2014) 192–198.
[45] M. Katriina, L. Teija, B. Kaj, The Effect of Nanoparticle Binders and Modified Precipitated Calcium Carbonate on Ink Absorption Behavior in a Multilayered Coating Layer, International Conference on Digital Printing Technologies and Digital Fabrication, The 32nd International Conference on Digital Printing Technologies (NIP): Printing for Fabrication 2016 : Materials, Applications, and Processes, 2016, pp. 457–460.
[46] H. Huang, X. Wang, H. Ge, M. Xu, Multifunctional magnetic cellulose surface-imprinted microspheres for highly selective adsorption of artesunate, ACS Sustainable Chem. Eng., 4 (2016) 3334–3343.
[47] W.H. Cheung, Y.S. Szeto, G. McKay, Intraparticle diffusion processes during acid dye adsorption onto chitosan, Bioresour. Technol., 98 (2007) 2897–2904.
[48] C.H.C. Tan, S. Sabar, M.H. Hussin, Development of immobilized microcrystalline cellulose as an effective adsorbent for methylene blue dye removal, S. Afr. J. Chem. Eng., 26 (2018) 11–24.
[49] C.H. Chan, C.H. Chia, S. Zakaria, M.S. Sajab, S.X. Chin, Cellulose nanofibrils: a rapid adsorbent for the removal of methylene blue, RSC Adv., 5 (2015) 18204–18212.
[50] H. Bensalah, M.F. Bekheet, S.A. Younssi, M. Ouammou, A. Gurlo, Removal of cationic and anionic textile dyes with Moroccan natural phosphate, J. Environ. Chem. Eng., 5 (2017) 2189–2199.
[51] G. Bayramoğlu, V. Cengiz Ozalp, M. Yakup Arıca, Removal of Disperse Red 60 dye from aqueous solution using free and composite fungal biomass of *Lentinus concinnus*, Water Sci. Technol., 75 (2016) 366–377.
[52] N. Maaloul, P. Oulego, M. Rendueles, A. Ghorbal, M. Díaz, Enhanced Cu(II) adsorption using sodium trimetaphosphate–modified cellulose beads: equilibrium, kinetics, adsorption mechanisms, and reusability, Environ. Sci. Pollut. Res., 28 (2021) 46523–46539.

Supplementary information

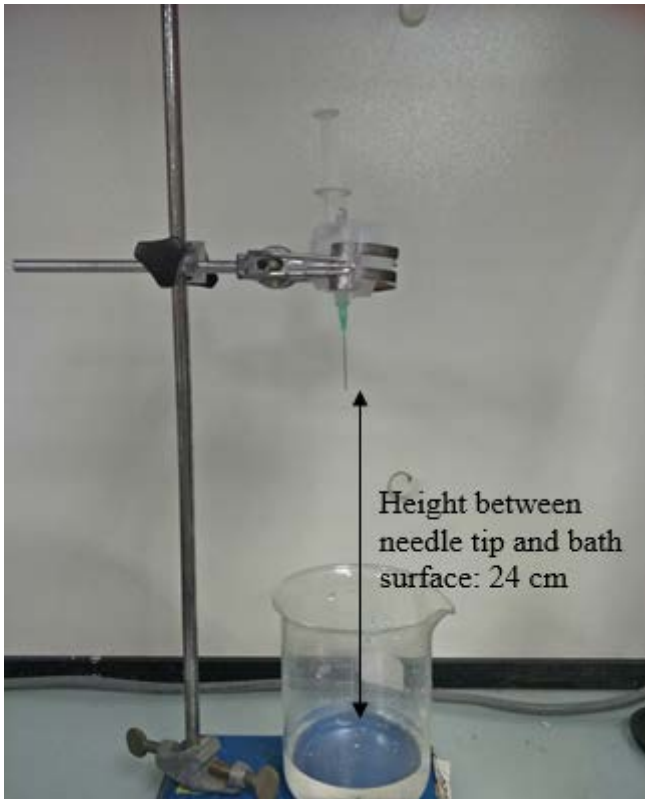

Fig. S1. Experimental set-up of the preparation of porous cellulose beads (PCBs) using $CaCl_2$ solution as the coagulation bath.

Table S1
BET surface area, pore volume and pore diameter for PCBs, PCBs/0.01 $CaCO_3$, PCBs/0.03 $CaCO_3$ and PCBs/0.05 $CaCO_3$

Sample	BET surface area (m^2/g)	Pore volume (cm^3/g)[a]	Pore diameter (nm)[b]
PCBs	2.67	0.0041	55.00
PCBs/0.01 $CaCO_3$	2.20	0.0044	13.34
PCBs/0.03 $CaCO_3$	1.95	0.0058	38.91
PCBs/0.05 $CaCO_3$	12.83	0.0103	7.15

[a]BJH adsorption cumulative volume of pore.
[b]BJH absorption average pore diameter.

Table S2
Absorption capacity at equilibrium (Q_e) and dye removal percentage for PCBs/0.07 $CaCO_3$

Sample	Q_e (mg/g)	Dye removal percentage (%)
PCBs/0.07 $CaCO_3$	43.87	90.94

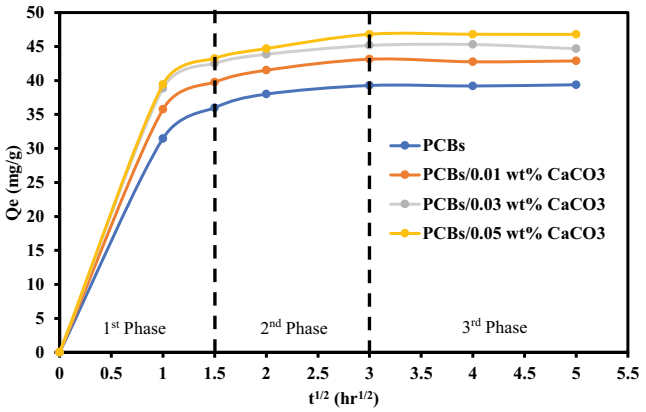

Fig. S2. Different phases of intraparticle diffusion model fitting on dye adsorption using PCBs with different $CaCO_3$ loadings.

Author Query

AQ1	Inline text citation for the Tables 4 and S1 is missing. Kindly provide the same.
AQ2	Reference citation order is not in sequence. So, we have changed the order and its Reference list. Kindly check.
AQ3	Kindly provide the Conference Location for the Reference [45].
AQ4	Tables 1 and S1 are looks same. Kindly check and update.
AQ5	Kindly provide the Manufacturer Location for the company “Sigma Life Science” “Merck”, “Sigma-Aldrich”, “Thermo Fisher Scientific Inc.”, “Hitachi Model TM3000”, “Micromeritics ASAP 2020”, “Cary 60, Agilent”, “Major Science, MS-NOR-30”.